A Indoor Positioning System of Bluetooth AOA Using Uniform Linear Array Based on Two-point Position Principle

Wenzhao Shu [1,2,2,2], Shuai Wang [3], Shuai Wang [3], and Qinghua Zhang [3]

[1]yanshan university
[2]Yanshan University
[3]Affiliation not available

October 31, 2023

Hosted file

16\begin{CJK}{UTF8}{gbsn}\end{CJK}\selectlanguage{english}(\selectlanguage{english}Rx).txt available at https://authorea.com/users/685514/articles/679333-a-indoor-positioning-system-of-bluetooth-aoa-using-uniform-linear-array-based-on-two-point-position-principle

An Indoor Positioning System of Bluetooth AoA Using Two-Point Position-Based Uniform Linear Array

Wenzhao Shu

***Abstract*— In recent years, there has been a significant rise in interest in indoor positioning research, with Bluetooth low energy (BLE) angle of arrival (AoA) positioning technology emerging as a prominent study area. This paper focuses on the Bluetooth AoA positioning system and proposes a 1D-multiple signal classification (MUSIC) algorithm that combines the principle of two-point positioning. This algorithm can be applied to linear, rectangular, and circular antenna arrays, leveraging In-phase(I) and Quadrature(Q) data to enhance positioning accuracy. The experiment is conducted in two steps. IQ samples are obtained from constant tone extension (CTE), which are then used to calculate the angle. Subsequently, the position of the tag is determined using mathematical plane relations. This study uses a uniform linear array (ULA) to solve AoA and two-point positioning (TPP) to determine the position of a label based on spatial geometric relationships between the two base stations and the label. Furthermore, we examine the feasibility of the positioning principle by conducting experiments in an open room, using three development boards and arrays of antenna boards to form a complete two-point positioning system. The experiments are conducted in line-of-sight (LoS) and non-line-of-sight (NLoS) environments within a laboratory measuring 12 m in length and 10 m in width. The obtained numerical values of the label positions exhibit an absolute error of 0.4–1.9 m achieved using the MUSIC algorithm, proving the practical feasibility of the two-point positioning.**

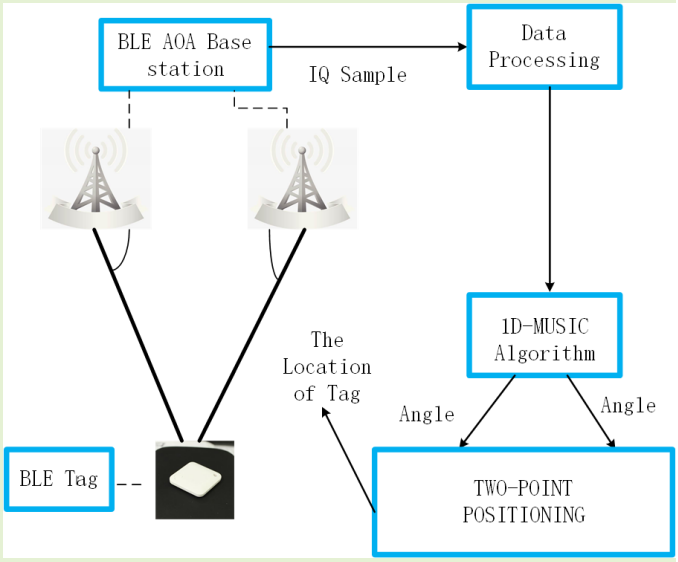

***Index Terms*— Bluetooth low energy, AoA, uniform linear array, CTE, IQ sample, MUSIC, two-point positioning.**

I. Introduction

THE positioning technology is crucial for several applications, and it can be categorized into indoor positioning and outdoor positioning based on the target area. Outdoor positioning technologies, such as global navigation satellite systems (GNSS) (for example, Russia's GLONASS, the European Union's GALILEO, and China's BDS), have been developed for many years and widely used [1]. However, indoor positioning remains a significant challenge due to the complex and diverse nature of the indoor environment [2], which includes walls, floor, and glass that block and reflect positioning signals. Therefore, applying GNSS to the indoor scene directly is not feasible. Given that a significant percentage of human activities occur indoors, the demand for indoor positioning technology is substantial, driving rapid advancements in this field [3], [4]. Numerous wireless technologies have emerged in indoor positioning, including WIFI, RFID, Zigbee, UWB, BLE [5], [6], and visible light [7]. Among these technologies, Bluetooth low energy (BLE) technology, which emerged with the introduction of Bluetooth 4.0 [8] and is characterized by low power consumption, has received considerable attention. Bluetooth dormancy allows Bluetooth devices to conserve energy by remaining dormant until necessary. This energy-efficient feature enables Bluetooth devices to operate for extended periods, typically 3–5 years, using a general coin cell battery. Consequently, BLE technology has become convenient for Bluetooth-based positioning applications [9].

Researchers worldwide have extensively studied angle of arrival (AoA) estimation. Below is a compilation of research conducted in the last three years. HajiAkhondi-Meybodi *et al.* [10] apply a convolutional neural network (CNN)-based indoor localization framework to track mobile agents with high accuracy in the presence of noise and Rayleigh fading channel. They verify the effectiveness of the proposed CNN-

The author is a master's student,coming form the Department of Mechanical Engineering, Yanshan University, Qinhuangdao City 066000, China (email: ysurobotswz@stumail.ysu.edu.cn.)

based AoA technique by using in-phase/quadrature (I/Q) samples modulated by gaussian frequency shift Keying (GFSK). Toasa *et al.* [11] evaluate the position of the Bluetooth low energy (BLE) transmitter based on the angle of arrival (AoA) mechanism proposed by the Bluetooth standard using software defined radio (SDR). Yen *et al.* [12] proposed the in-phase(I) and quadrature(Q) density-based AoA estimation (IQDAE) algorithm and applied phase difference (PD) filter to enhance the accuracy of angle calculation by incorporating a uniform linear array (ULA). Hajiakhondi-Meybodi *et al.* [13] designed the switch antenna array (SAA) model and applied the nonlinear least square (NLS) curve fitting and gaussian filter (GF) methods to enhance the accuracy of IQ values in conjunction with Texas Instruments' AoA positioning antennas. In their study, Mohaghegh *et al.* [14] introduce a novel and efficient antenna array with fast switching capabilities designed for BLE direction finding, by implementing our newly designed antenna array and switch, and achieve an accuracy of around 5°. Paulino *et al.* [15] present a system topology and algorithms for self-localization, in which a receiver with an antenna array utilizes the AoAs from fixed battery-powered beacons to self-localize without a centralized system or wall-power infrastructure. They achieve a mean absolute error of 3.6 m in position estimations and compute the AoA with an root mean squared error(RMSE) of 10.7°. Xiao *et al.* [16] theoretically analyze the performance degradation of AoA estimation caused by phase noise. They also propose an EM-MUSIC algorithm that utilizes an extended kalman filter to estimate the phase noise and improve the accuracy of AoA estimation. These researchers have made certain contributions to AOA research, but their research also has shortcomings in two main aspects. Firstly, the signals they study are mainly computer-simulated or SDR signals, which cannot reflect real-life situations. As a result, this method has certain limitations. Secondly, most of the previous work involves only the estimation error of AOA, measuring the angle error without applying it to positioning applications. This limitation does not reflect the high-precision characteristics and applications of AOA positioning.

Bluetooth technology operates in the 2.4-GHz industrial, scientific, and medical (ISM) band, which is also shared with other signals, such as WIFI, leading to potential interference. The Bluetooth bandwidth spans about 80 MHz and can be divided into 40 channels, each occupying the 2-MHz bandwidth. These channels are categorized into three broadcast channels and 37 data channels, each serving a distinct role. Bluetooth AoA positioning adopts connection and connectionless modes [17]. The connection mode facilitates data exchange using the data channels, employing frequency hopping technology to mitigate external interference. Connectionless mode enables direct broadcast functionality, providing positioning capabilities for multiple labels.

Bluetooth positioning relies on two principles: received signal strength (RSS) [18] and direction of arrival (DoA) [19]. RSS-based positioning operates assuming that the signal strength decreases as the path of the received signal in space increases. Previous research has established mathematical models to represent the signal strength in relation to the distance. Another approach involves constructing a database with fingerprint data from various points in space, enabling and identifying unknown points based on their RSS values. In contrast, DoA uses phase differences observed when signals reach different antennas to estimate angles using the spatial spectrum estimation algorithm [20]. These angles typically include azimuth and elevation [21]. While previous studies focus on simulating signals using MATLAB software and estimating angles, they disregard the real hardware conditions. Therefore, this study is the first to explore the IQ of constant tone extension (CTE) and the construction of the signal matrix. We employ IQ numerical signal processing and the one-dimensional MUSIC algorithm for real-world AoA scenarios, going beyond the scope of previous research. In addition, we also use the two-point positioning principle to examine the development of an indoor positioning system.

We propose a localization algorithm to determine the position of a label based on the two-point positioning (TPP) principle. Before applying the TPP calculation, we use the MUSIC algorithm [22], [23] to solve the azimuth of the tag. Consequently, the positioning system can be represented by a two-step process. First, we construct a coordinate system for the respective positions of the tag and the base station, assuming that the two base stations are on the coordinate axes. Next, we establish the relationship between the known azimuth and the coordinates by using the trigonometric function expression and solving the matrix equation to determine the position of the label [24].

This paper utilizes the Bluetooth 5.1 principle to construct a hardware-based Bluetooth AOA positioning system. It aims to validate the feasibility of Bluetooth AOA positioning through the two-point positioning principle. The key contributions of this paper are as follows:

1) Using the principle of Bluetooth 5.1, a Bluetooth AOA positioning system was developed. This system employed a Nordic development board and a rectangular antenna array to confirm the practicality of Bluetooth 5.1 direction finding.
2) The IQ value is obtained from real-world conditions and can be affected by noise, which reflects a more realistic application scenario compared to using simulated computer data. This approach ensures the credibility of the experiment.
3) The extracted IQ data underwent data processing, and an algorithm was developed to verify the angle error of AOA. Additionally, a TPP algorithm was proposed and applied to estimate the position of the labels.
4) The comparison experiment between line-of-sight and non-line-of-sight positioning errors is conducted in the indoor space. It demonstrates higher accuracy when compared to WIFI and other positioning methods. The discussion of the factors that influence positioning errors under non-line-of-sight conditions offers valuable insights for future Bluetooth applications.

The remainder of the paper is structured as follows. Section II describes the principle of the BLE AoA positioning. Section III discusses the MUSIC algorithm, the TPP principle, and

the solution expression for position estimation. Section IV elaborates on how we process IQ data and obtain the position solution. Section V illustrates the experimental results of using boards to locate the tag. Finally, Section VI concludes the paper based on our research findings.

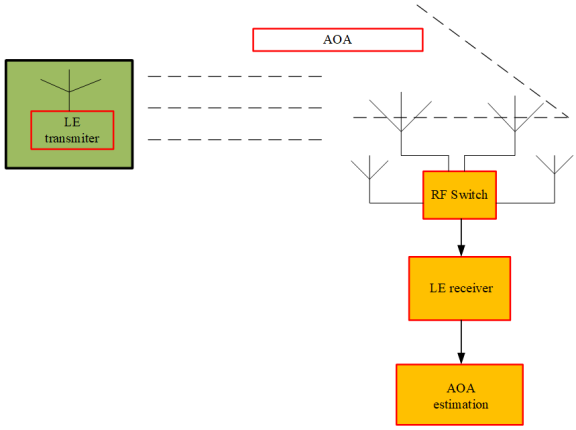

Fig. 1: BLE AoA positioning structure. The transmitter transmits the signal at the same time as the receiver receives samples through the RF switch-controlling antenna, and the values sampled by the spatial spectrum algorithm are used to estimate the AoA.

II. AoA Principle

The Bluetooth AoA positioning system structure (Fig. 1) primarily comprises three components a transmitter, a receiver, and an antenna array with radio frequency (RF) switch.

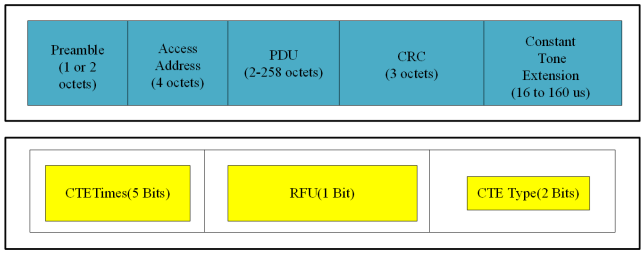

Fig. 2: CTE packet structure. The transmitter transmits the BLE packet, including CTE, which is the RF sinusoidal signal at the end of the packet. The CTE can be demodulated to IQ samples.

A. CTE and IQ samples

The CTE [25] (Fig. 2) is a set of extension packets with a series of unwhitened packets added to the Bluetooth broadcasts for Bluetooth direction finding, with the packets' lengths varying from 16 μs to 160 μs. The CTE primarily comprises the guard period, reference period, and switch-sample period [26]. The guard and reference periods have fixed periods of 4 μs and 8 μs, respectively. The switching sampling period relies on the length of an antenna array. The sampling period can be subdivided into 1 μs and 2 μs, equal to the time of the switching period; the sampling and switching operations are held sequentially. For example, if there are 12 sampling antennas and the sampling period is set to 1 μs, the length of the switch-sample period would be 24 μs.

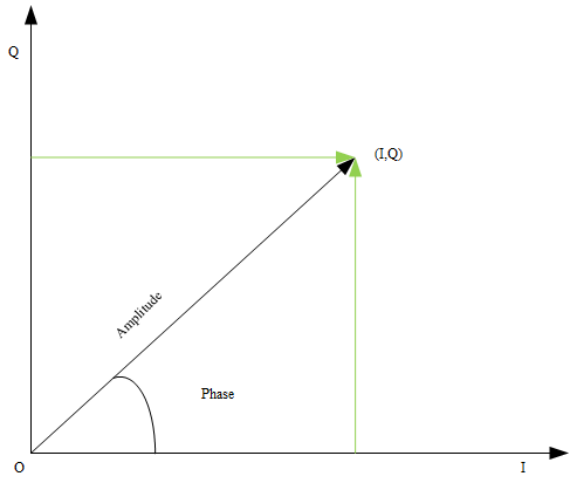

Fig. 3: The relation of the original signal and I/Q. There are two axes here, the I axis and the Q axis. The vector Amplitude and arc Phase represent the signal amplitude and phase, respectively, expressed by IQ according to the mathematical relationship.

CTE can be classified into AoA and angle of departure (AoD) according to the CTEType. According to Bluetooth protocol 5.1, AoA is enabled by default in the configuration, while AoD is divided into two subtypes: AoD 1 μs and AoD 2 μs. When CTE passes through the antenna array, it is decomposed into I (in-phase) and Q (quadrature) (Fig. 3), whose mathematical relationship can be expressed by (1) and (2). The amplitude and phase of the signal are the sum of the squares and the tangent ratio of Q and I, respectively. If the expression of the signal is $A\sin(\theta)$, and IQ is the value of its two orthogonal signals, the following formula [25] can be obtained

$$A = \sqrt{I^2 + Q^2} \tag{1}$$

$$\theta = \arctan\frac{Q}{I} \tag{2}$$

where A and θ denote the signal's amplitude and phase angle (unit angle), respectively. I and Q represent the values of the two signals after sampling.

B. Antenna Array

Two roles in Bluetooth device connection in BLE 4.0 are the master and the slave. However, with the advent of BLE 5.0, these roles have been transitioned to central and peripheral devices. The I/Q data is sampled by the antenna array, a collection of distinct antennas. The antenna arrays can be categorized into linear and plane arrays per their shapes. A linear array is a group of antennas arranged at equal intervals. It is one-dimensional and is commonly used for plane angle estimation calculations. In contrast, plane arrays are two-dimensional and can be used to estimate azimuth and elevation. Plane arrays are subdivided into circular and square arrays. The antenna

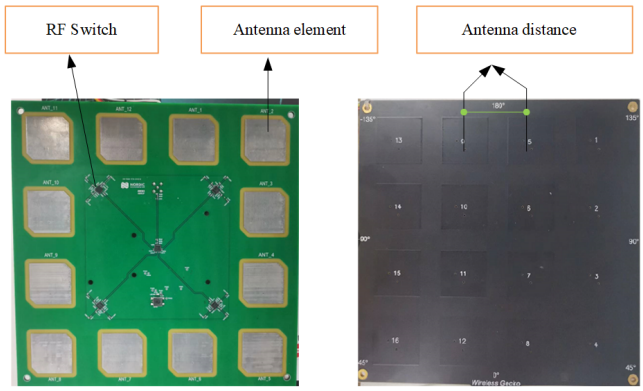

Fig. 4: Two types of antenna array. The rectangles on the left and right represent antennas, with spacing between them. Both antenna arrays have their RF own switch, which can control the antenna switching.

boards of Nordic and SiliconLabs (Fig.4) [27] are square array antenna boards. Nordic's antenna boards are numbered, starting from the upper left corner with the number 11, and circulating clockwise, followed by 12, 1, 2, until the 10^{th} antenna, totaling 12 antennas. Similarly, SiliconLabs' antenna boards start from the upper right with the number 1, increasing sequentially until 16, totaling 16 antennas. The only difference is that Nordic has four antennas removed in the middle; however, there is no difference between the angle calculations of the two.

The antenna board is controlled by an RF switch that uses a gate logic circuit to combine binary digits (0 and 1) for controlling multiple antennas. The antenna switching process is regulated by four general-purpose inputs/outputs (GPIOs) (Fig. 5). These GPIOs can control 16 digital states through various logical combinations. Each digital state corresponds to an antenna-switching switch, and the logic level of the respective GPIO pins determines the antenna-switching control.

Antenna switching is controlled by the antenna pattern (Table.I). For example, when the switched antenna is No. 12, its logic level is 0b0000, indicating that all four controlled pins are set to a low-level state. This pattern holds for other antennas as well. By comparing the logic analyzer diagram (b), the antenna switching can be verified according to the specified antenna pattern.

TABLE I: The antenna-switching pattern (partial)

Antenna	Pattern [3:0]
ANT11	0b0010
ANT12	0b0000
ANT1	0b0101
ANT1	0b0110

C. AoA Calculation

AoA calculation in the system is defined by the principle of phase difference (PD) [28]. Assuming the signal is a plane wave and the array antenna is a linear array, there will be a

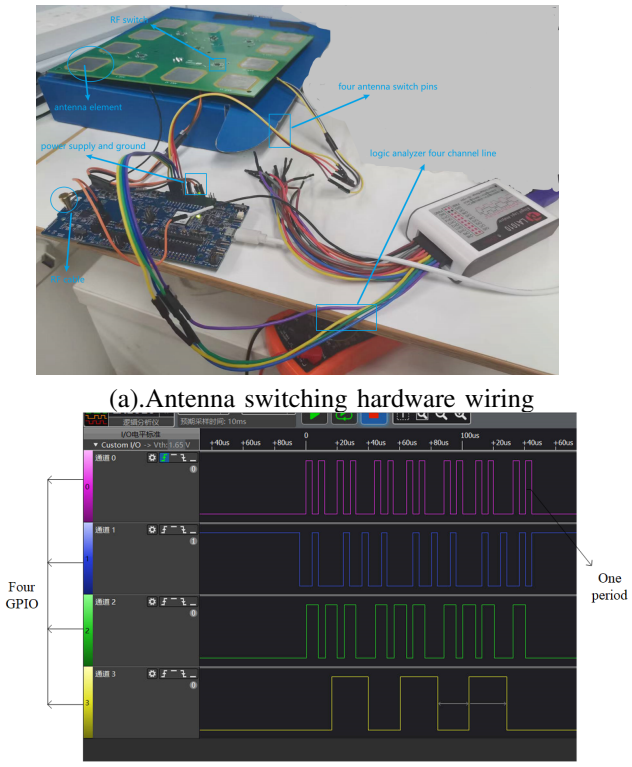

(a).Antenna switching hardware wiring

(b).The logic level of antenna switching

Fig. 5: Antenna array switching verification. (a). There are four antenna pins to control each of the four channels of the logic analyzer. (b). Each channel reflects the current logic level of the corresponding switching antenna, a group of four levels.

phase difference between two adjacent antennas because the time taken for the signal to reach different antenna elements varies (Fig. 6). First, the respective phases of antennas A and B are computed using (2). As there exists a distance difference between the signal reaching antenna A and antenna B, this distance is calculated following the electromagnetic wave theory. Subsequently, the triangular relationship and the cosine function [29] can be used to determine the angle and distance as follows:

$$D\cos(\theta) = \frac{\Delta\varphi\lambda}{2\pi} \tag{3}$$

This deformed expression is solved for the angle value using the inverse cosine function, as shown:

$$\theta = \arccos\left(\frac{\Delta\varphi\lambda}{2\pi D}\right) \tag{4}$$

where θ is the AoA, D is the distance of two adjacent antennas, λ is the wavelength of the received signal, and $\Delta\varphi$ is the antennas' phase difference.

III. AoA Algorithm and TPP Theory

A. 2-D MUSIC algorithm

We propose the following assumptions to explain the AoA algorithm:

1. Although there may be multiple signal sources, this paper considers only one signal source, referred to as the tag.

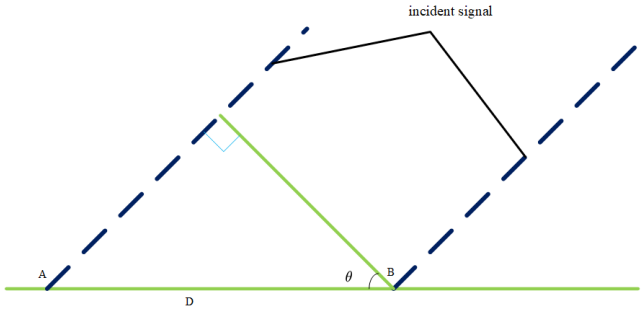

Fig. 6: AoA phase difference axiom. Since there is a time delay between the arrival of plane waves at two antennas, AoA can be calculated from the phase difference of adjacent antennas.

2. The signal is assumed to be a narrowband signal, and the distance D between the antennas is less than half the wavelength of the signal ($\frac{\lambda}{2}$).

3. External interference, such as multipath and emission effects caused by objects, including walls and glass, are absent. However, additive Gaussian white noise (AGWN) is considered the noise factor.

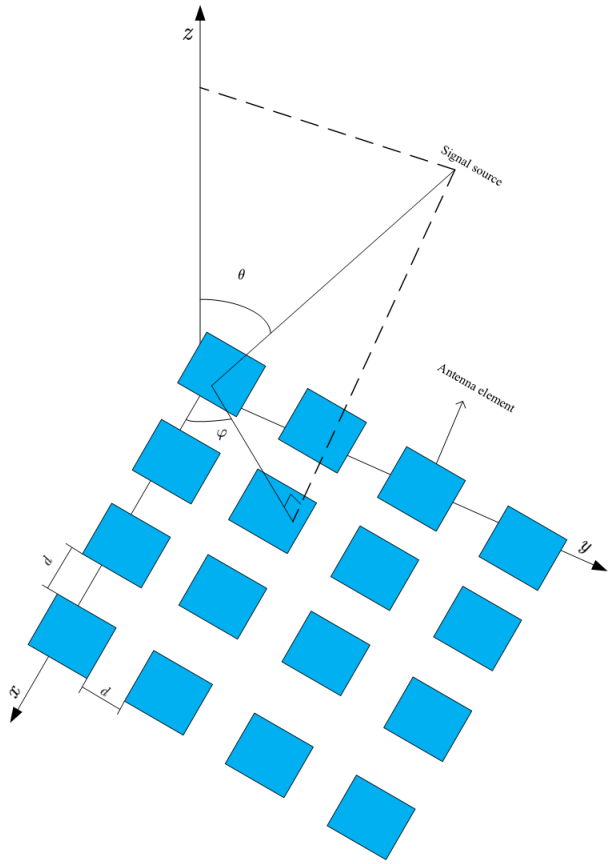

Fig. 7: The model of AoA array antenna in URA. The array antenna model is made of 16 antennas. The antennas are equally spaced, and the arrays are in a 4x4 shape. Two angles can be calculated using this model.

Fig. 7 illustrates the mathematical model of AoA estimation, where the θ and ϕ represent elevation and azimuth, respectively. dx and dy denote the spacing between the antennas on the x-axis and y-axis, respectively, with both distances being equal.

A planar array is a multi-dimensional extension of a linear array; therefore, we can decompose this model into linear arrays in both directions. Since the x-direction and y-direction arrays are parallel, we analyze only one direction. Assuming the mathematical expression of the signal is $A\sin(\varphi)$, the actual calculation can be performed by the I/Q data. The antenna array type used is a uniform rectangle array (URA) with M by N dimensions, where M and N represent the numbers of antenna elements on the x-axis and y-axis, respectively. The reference point selected is the reference antenna, and therefore, the distance of the first antenna [30] on the x-axis relative to the first antenna is $(k-1)dx$. Consequently, the antenna transpose vector can be represented as $a_x(\theta,\phi) = e^{(-j2\pi(k-1)dx\sin(\theta)\cos(\phi))}$ and $a_y(\theta,\phi) = e^{(-j2\pi(k-1)dy\sin(\theta)\sin(\phi))}$ for the x axis and y axis, respectively. With these considerations, the following can be derived

$$a_x(\theta,\phi) = [1,\cdots,e^{(-j2\pi(M-1)dx\sin(\theta)\cos(\phi))}]^T \tag{5}$$

$$a_y(\theta,\phi) = [1,\cdots,e^{(-j2\pi(N-1)dy\sin(\theta)\sin(\phi))}]^T \tag{6}$$

Since we consider a single incoming signal, the direction matrix and direction vector of the array elements are equal. We denote A_x and A_y as the orientation matrices in the x-direction and y-direction, respectively, and obtain the [31]following

$$A_x(\theta,\phi) = [1,\cdots,e^{(-j2\pi(M-1)dx\sin(\theta)\cos(\phi))}]^T \tag{7}$$

$$A_y(\theta,\phi) = [1,\cdots,e^{(-j2\pi(N-1)dy\sin(\theta)\sin(\phi))}]^T \tag{8}$$

For the x-axis subarray, the received signal is

$$x_x(t) = A_x s(t) + n_x(t) \tag{9}$$

For the y-axis subarray, the received signal is

$$x_y(t) = A_y s(t) + n_y(t) \tag{10}$$

The $n_x(t)$ and $n_y(t)$ represent the AWGN of the x-axis and y-axis, respectively.

The whole output signal $x(t)$ is expressed by $x_x(t)$ and $x_y(t)$ as follows

$$x(t) = [A_x \odot A_y]s(t) + n(t) \tag{11}$$

where $A_x \odot A_y$ represents the Khatri-Rao product [32] of A_x and A_y. Therefore, we obtain $A_x \odot A_y = A_x \otimes A_y$, where $\otimes$ denotes the Kroecker product of two matrices. The above equation transforms to

$$\begin{matrix} A_x \\ \otimes \\ A_y \end{matrix} = \begin{bmatrix} 1,\cdots,e^{(-j2\pi(N-1)dy\sin(\theta)\cos(\phi))},\cdots \\ e^{(-j2\pi dx\sin(\theta)\sin(\phi))}e^{(-j2\pi(M-1)dx\sin(\theta)\sin(\phi))},\cdots, \\ e^{(-j2\pi((M-1)dx\sin(\theta)\sin(\phi)+(N-1)dy\sin(\theta)\cos(\phi)))} \end{bmatrix} \tag{12}$$

where $A_x \otimes A_y$ is $MN \times 1$ matrix. Using (12), the covariance matrix R_{xx} of the signal can be constructed. The spatial spectrum algorithm determines the signal subspace and the noise subspace to be orthogonal. After decomposing the

covariance matrix and sorting the eigenvalues in ascending order, the covariance matrix can be expressed as a signal subspace and the noise subspace as follows

$$R_{xx} = E[x(t) * x(t)^H] \tag{13}$$

$$R_{xx} = U_S \sum_S U_S + U_N \sum_N U_N \tag{14}$$

where E and H denote the mean and conjugate transpose of the matrices, respectively. U_S and U_N indicate the signal and noise space eigenvector, $\sum_S$ and $\sum_N$ represent the signal and noise space eigenvalue, respectively. The spectral function is expressed as follows

$$P_{MUSIC} = \frac{1}{A(\theta,\phi)^H U_N U_N^H A(\theta,\phi)} \tag{15}$$

Using the space search method, we can locate the spectral peak, and the corresponding angle represents the direction of the target signal. Only one direction is considered for linear arrays, and the rest of the calculation is the same as the two-dimensional algorithm. Therefore, further derivation is not illustrated in this paper.

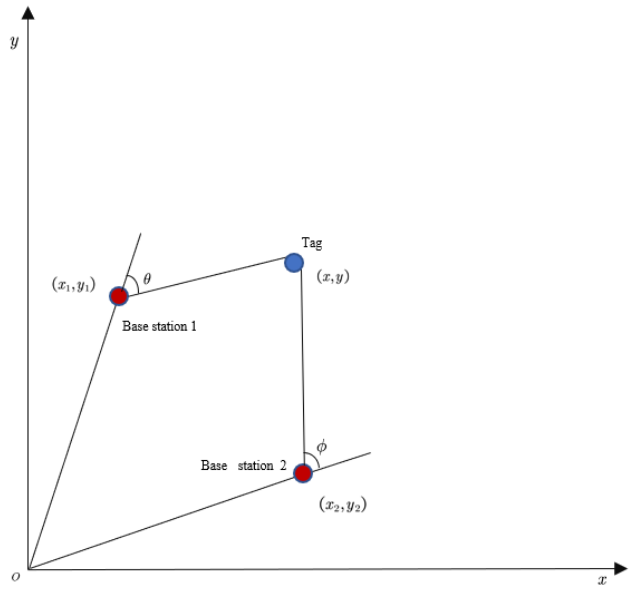

Fig. 8: The calculation principle of two-point positioning. The two base stations can get the angles from the same tag, and then the tag position can be calculated by trigonometric function.

B. Two-Point Positioning Principle

Based on the previous analysis, we can use the AoA algorithm to compute the angle. Referring to Fig. 8, we assume that the intersection angle between the first base station and the tag is θ, and its coordinates are (x_1, y_1). Similarly, the other base station has an intersection angle and coordinates of ϕ and (x_2, y_2), respectively. We assume that both angles are not equal to 90°. Since the base station coordinates are known, we can establish the expression of coordinates of the label at (x, y) using the trigonometric function relationship and known angles. In this study, the base station is placed on the y-axis and the x-axis, respectively, to facilitate the calculation.

For base station 1, the relationship can be established using the tangent value as follows

$$tan\theta = \frac{y - y_1}{x - x_1} \tag{16}$$

For base station 2, the same expression can be obtained as

$$tan\phi = \frac{y - y_2}{x - x_2} \tag{17}$$

By expanding the above equations, we can isolate the left side of the label's coordinate value, and the right side represents the coordinate values of the base station, as shown by the following matrix equation

$$\begin{bmatrix} 1 & -\tan\theta \\ 1 & -\tan\phi \end{bmatrix} \begin{bmatrix} y \\ x \end{bmatrix} = \begin{bmatrix} y_1 - x_1\tan\theta \\ y_2 - x_2\tan\phi \end{bmatrix} \tag{18}$$

By using the inverse of the matrix, the position of the tag can be calculated as follows

$$\begin{bmatrix} y \\ x \end{bmatrix} = \begin{bmatrix} y_1 - x_1\tan\theta \\ y_2 - x_2\tan\phi \end{bmatrix} \begin{bmatrix} 1 & -\tan\theta \\ 1 & -\tan\phi \end{bmatrix}^{-1} \tag{19}$$

When the base station is not in a special location, establishing two equations based on the relationship between the tag and the base stations is possible using quadrilateral calculations. We can then use the mathematical relationship to solve these equations. Further reasoning is not provided in this study.

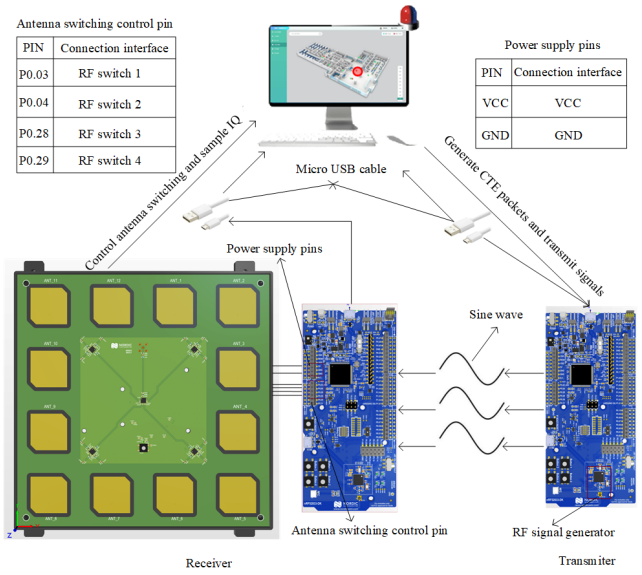

Fig. 9: Bluetooth AoA positioning system. The system consists of two Nrf52833dks and an antenna board, and the one with the antenna array is the receiver. The transmitter and the receiver are powered through a serial cable, and the receiver receives IQ data from the serial port.

IV. Data Processing and Position Calculation

This chapter describes the experimental setup using the Nrf52833dk development board from Nordic (Fig. 9). Nordic's rectangular antenna board comprises 12 antennas. The processing involves two aspects. First, the acquired IQ values are normalized and digitally processed to obtain signal amplitude and phase. Second, the phase is used to calculate the angle via the one-dimensional MUSIC algorithm, followed by the two-point positioning algorithm to determine the position.

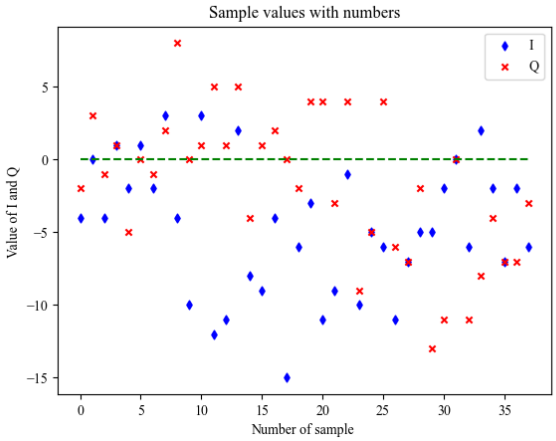

Fig. 10: The original IQ samples. The blue and red dots carry the I and Q values of the IQ sample, respectively, where the green dotted line represents the size relationship between IQ and 0, so the distinction is made for phase calculation.

A. Data processing

A linear array is used for the two-point positioning. Referring to Fig. 4, we use antennas 11 (A_{11}), 12 (A_{12}), 1 (A_1), and 2 (A_2). Antenna 11 is the reference antenna, which does not require switching. Antennas 12, 1, and 2 are sampling antennas used for switching and sampling the IQ values multiple times; their CTE length is 72 μs. The sampled IQ sample had the software-defined cycle period and the number of sampling cycles of 60 μs and 10, respectively. The phase value can be calculated, but it has tangent value limitations. When the angle is located in the first or third quadrant, the tangent value of the calculated angle is the same, but the actual angle is different. In addition, if the value of I is zero, it cannot be calculated directly from the formula. The classification of different IQ values with zero is illustrated in Fig. 10, and the derived expression is as follows

$$\varphi(Q,I)=\begin{cases}\arctan\frac{Q}{I}+\pi & (I<0)\\ \arctan\frac{Q}{I} & (I>0,Q\geq 0)\\ \arctan\frac{Q}{I}+2\pi & (I<0,Q<0)\\ \frac{\pi}{2} & (I=0,Q>0)\\ \frac{3\pi}{2} & (I=0,Q<0)\end{cases} \tag{20}$$

After calculating IQ values, the phase values are corrected. Since the original sinusoidal signal has a period of 2 μs, the calculated value of the subsequent antenna sampling should be greater than the previous one. The calculation algorithm [33] (Algorithm 1) processes the data to obtain the absolute phase difference. Subsequently, we acquire 38 groups of all phase values that increase according to the specified phase. The amplitude of the collected signal is also simultaneously calculated.

B. Angle Conclusion and Position Solution

Algorithm 1: The phase increasing algorithm

```
// Define the phase increasing function
def function phase-increasing[φ_ref]:
// Counter variable count
    count = 0;
// Loop through phase angles
    for i in range(2, len(φ_ref)):
// Determine the relationship between adjacent phase angles
        if φ_ref(i) ≤ φ_ref(i−1):
            count += 1
// Get new phase value again
        φ_ref(i) = φ_ref(i−1)+count*2π
        else:
            continue
end
```

According to the equation (5–8), the spacing between the antenna elements is significantly important. Therefore, we choose the center of the reference antenna as the origin to establish a coordinate system. Following the antenna technical manual of Nordic company, the antenna spacing D is 40 mm. Subsequently, the x coordinates of the antennas 11, 2, 1, and 2 are determined to be 0, 0.04, 0.08, and 0.12, respectively. The obtained phases and amplitudes are recorded as $\varphi_1, \cdots, \varphi_{38}$ and $Am_1, \cdots, Am_{38}$ according to the sampling order. The calculation involves using the sampling antenna while excluding the samples from the initial reference antenna(antenna 11). The extraction is performed in the same antenna iteratively, constructing the phase and amplitude vectors as follows

$$\varphi_{all}=[\varphi_1,\varphi_2,\cdots,\varphi_{37},\varphi_{38}] \tag{21}$$

$$Am_{all}=[Am_1,Am_2,\cdots,Am_{37},Am_{38}] \tag{22}$$

For example, the first antenna sample starts from serial number 9, and the number of loop antennae is 3. We can extract the phase and amplitude of the same antenna data as shown

$$\varphi_{12}=[\varphi_9,\varphi_{12},\varphi_{15},\varphi_{18},\varphi_{21},\varphi_{24},\varphi_{27},\varphi_{30},\varphi_{33},\varphi_{36}]^T \tag{23}$$

$$Am_{12}=[\begin{matrix}Am_9,Am_{12},Am_{15},Am_{18},Am_{21}\\,Am_{24},Am_{27},Am_{30},Am_{33},Am_{36}\end{matrix}]^T \tag{24}$$

We construct the signal $s(t)=Ae^{-j*\phi}$ using the obtained amplitude and phase. Considering the first antenna, the steering vector of the antenna can be acquired. Assuming that the plane angle is θ, its vector can be represented as $e^{-j*2\pi*0.04}$. Consequently, the output matrix of the first antenna is

$$x_1=[Am_9e^{-j\varphi_9}e^{-j0.08\pi},\cdots,Am_{36}e^{-j\varphi_{36}}e^{-j0.08\pi}]^T \tag{25}$$

$$x = \begin{bmatrix} Am_9 e^{-j\varphi_9} e^{-j0.08\pi}, \cdots, Am_{36} e^{-j\varphi_{36}} e^{-j0.08\pi} \\ Am_{10} e^{-j\varphi_{10}} e^{-j0.16\pi}, \cdots, Am_{37} e^{-j\varphi_{37}} e^{-j0.16\pi} \\ Am_{11} e^{-j\varphi_{11}} e^{-j0.24\pi}, \cdots, Am_{38} e^{-j\varphi_{38}} e^{-j0.24\pi} \end{bmatrix} \tag{26}$$

By extending this process to other antennas are processed, we can form the final output of 3 by 10 matrix. The matrix is then averaged, and the singular value decomposition is performed. The noise vector is obtained from the last row of the covariance matrix. Using the spectral function, we assume that the angle varies from 0° to 180°, and the direction angle can be determined by finding the maximum value using an extreme value search.

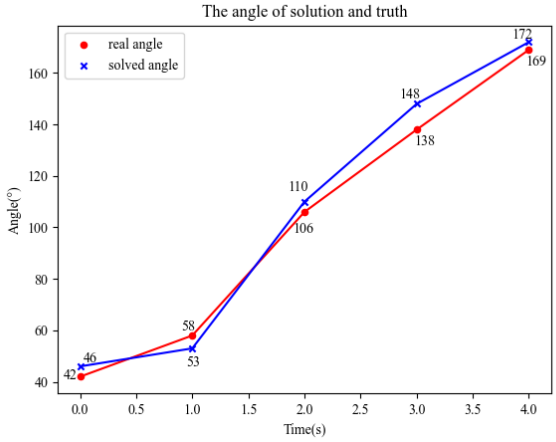

Fig. 11: The angles between the true position and solution by the algorithm. The true angles are 42°, 58°, 106°, 138°, and 169°, and the angles of solution are 46°, 53°, 110°, 148°, and 172°. The difference between both angles is insignificant.

In this case, five positions are selected, and their angles are solved using the one-dimensional MUSIC algorithm. The real position angle and the angle solved by the algorithm (Fig. 11) demonstrate that the difference between the maximum and minimum angles ranged from 3° to 10°. This finding indicates that the algorithm can solve the azimuth angle between the tag and the base station with high accuracy.

V. Experiment and Analysis

We conducted the experiment (Fig. 12) in the center of a room with a length and width of 12 m and 10 m, respectively. According to the two-point positioning method, we put the two base stations and tag on the same horizontal plane. Both the tag and the base station are placed on a tripod, 1.2 meters above the ground. Base station 1 is placed on the y-axis, 5 m away from the origin, while base station 2 is placed on the x-axis, 6 m away from the origin. Environments are divided into line of sight (LoS) and non-line of sight (NLoS). Both base stations are equipped with antenna arrays, while the tag does not have antenna arrays. We place the labels in four different positions (3.7,2.5), (5.7,4.6), (7.5,6.2), and (9.5,8.3). The algorithm is then used to solve these positions in both environments. Each position is calculated five times, and the average is taken. In the LoS environment, the solution coordinates are (2.3,3.1), (6.2,5.0), (6.8,6.7), and (11.1,9.3). In contrast, in the NLoS environment, the solution coordinates are (1.8,3.5),(6.6,5.3),(6.4,6.8), and (11.4,9.1). Subsequently, we calculate the absolute errors in the x and y directions (Fig. 13) in both environments. The errors in the LoS and NLoS environments range from 0.4 to 1.6 m and 0.6 to 1.9 m, respectively. Finally, we compute the average errors of x and y and obtain their average. The results indicate the LoS and NLoS errors to be 1.2 m and 1.6 m, respectively. There are two findings from the test results. Firstly, the accuracy increases and the error in the two coordinate axis directions decreases as the absolute distance between the tag and the two base stations decreases. This is due to the longer distance traveled by the electromagnetic waves, which takes longer based on the switching of electromagnetic waves and antenna arrays. However, the control of the antenna array is at a subtle level and the actual IQ value of the collected signal may not correspond to the current antenna switching, resulting in IQ error. Consequently, the error in AOA is larger in distant places. Secondly, in a NLoS environment, the positioning accuracy is lower. This is because the signal is either absorbed or reflected when it encounters blocking objects such as glass and metal during NLoS propagation. As a result, the collected IQ data becomes inaccurate, leading to a greater AOA angle error and ultimately increasing the positioning error.

In addition, the one-dimensional MUSIC and TPP algorithms are determined to calculate the position of the label effectively. The error range in x and y-coordinates is 0.4–1.9 m. The positioning accuracies of Bluetooth RSSI and WIFI are 3.5 m and 4 m, respectively (Table.II). Compared with pressing AoA, the positioning accuracy is two to three times lower. Besides the localization accuracy, the method proposed in this paper has other advantages. First of all, Bluetooth AoA requires only two base stations for localization, which reduces costs and deployment workload compared to WIFI and Bluetooth RSSI, which require three base stations. Secondly, in terms of positioning principles, WIFI and Bluetooth RSSI use RSSI values, which are unstable and highly influenced by the environment. In contrast, Bluetooth AoA utilizes IQ values obtained through antenna arrays and Bluetooth-specific data packets, thereby significantly enhancing positional stability. Consequently, Bluetooth AoA positioning is more reliable. Finally, in terms of industrial deployment, WIFI fingerprint positioning necessitates two stages: offline collection and online verification, which consume substantial time, cost, and effort. Conversely, Bluetooth AoA only requires on-site data collection and coordinate resolution, reducing workload significantly. This reduction in workload is an advantageous aspect that should not be overlooked. Therefore, Bluetooth AoA is considered a high-precision positioning technology.

Although the Bluetooth AOA positioning we proposed has the advantage of high positioning accuracy, its technology also has some shortcomings. One of the main challenges lies in guaranteeing the precise control of array units due to the involvement of antenna arrays. This may introduce significant difficulties during implementation. Additionally, the AOA technology heavily relies on IQ data, leading to

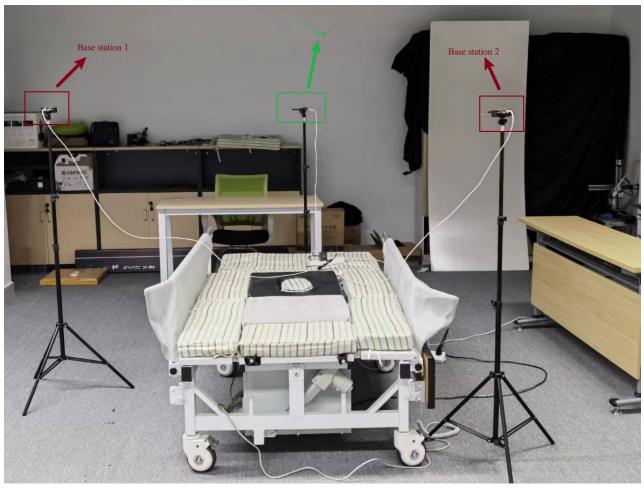

(a) **Model in LoS (ideal model)**

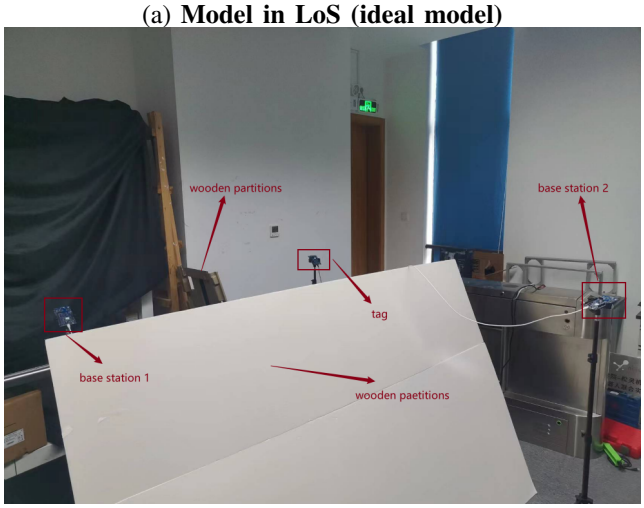

(b) **Models in NLoS**

Fig. 12: Experimental models in LoS and NLoS environments. (a). Under the idealized model, there is no object blocking between the base station and the tag, and the signal transmitted from the tag to the base station does not cause interference. (b). In an NLoS environment, the two base stations and the tags are blocked by a wooden board, and the signal will be reflected or scattered. This state is a real state.

a substantial consumption of resources when running the AOA algorithm. Such resource consumption is considered a drawback. Furthermore, since Bluetooth signals and WiFi signals overlap, there is a need to improve the interference avoidance mechanisms in this area.

Due to the high accuracy of the 1-D MUSIC algorithm calculation, the corresponding angles are calculated, enabling the computation of the label's position through the two-point positioning method.

TABLE II: Precision of two positioning methods (Area range of 12 m x 10 m)

Positioning Method	Precision
Bluetooth RSSI	3.5 m
WIFI	4 m

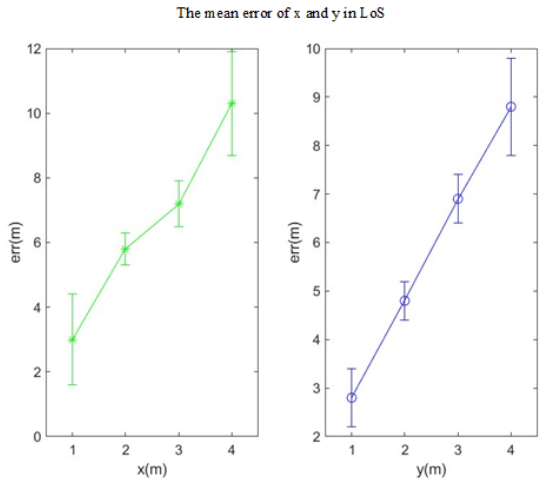

(a) **Error of x and y directions in LoS**

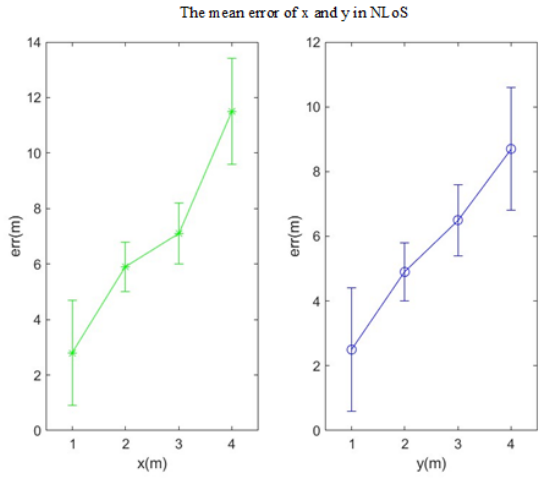

(b) **Error of x and y directions in NLoS**

Fig. 13: Error in the direction of the two axes in the two environments. In the NLOS environment, the errors are greater than those in the LOS direction. The error is in the range of 0.4–1.9 m; the closer the tag is to the base station, the smaller the error is.

VI. Conclusion

In this paper, we developed a Bluetooth AOA positioning system using the Bluetooth 5.1 positioning principle. The system consists of two base stations equipped with matrix antenna arrays and one tag. To transmit signals from the tags, we utilized the software SDK, which allowed the base station to receive and process the I/Q data. The IQ phase correction was conducted, resulting in an updated IQ value. We employed the MUSIC algorithm to solve AOA, comparing the AOA error to determine if it falls within the acceptable range of error. Furthermore, we conducted positioning accuracy tests based on the two-point positioning principle in both line-of-sight and non-line-of-sight scenarios. The results demonstrated that Bluetooth AOA positioning accuracy was in the meter-level range, confirming its reliability as a positioning technology. Additionally, a comparison with WIFI technology revealed that Bluetooth AOA technology has several advantages, such

as high precision, low cost, and low power consumption. However, the research also highlighted the limitations of Bluetooth AOA technology.

Compared with previous research, our research holds certain significance. Most traditional AOA estimates utilize computer-simulated data or Bluetooth data packets simulated by SDR. These data lack real-world environment and do not include noisy data, thus diminishing their persuasiveness in practical applications. Furthermore, previous explanations of DOA estimation were limited to the perspective of AOA without practical implementation. AOA technology, however, is ultimately intended for positioning. In our study, we not only apply AOA technology to practical use through two-point positioning, but also demonstrate its technological superiority. It is crucial to promote, apply, and further research this technology, ultimately leading to the development of products that serve the needs of humanity. Although the plane positioning we achieved is only a foundation, it offers insights for three-dimensional or local positioning. Moreover, the demand for indoor positioning is increasing in various aspects of daily life, such as smart parking where traditional positioning techniques fall short in accuracy. While UWB technology was once regarded as a promising solution, high cost recently emphasized that Bluetooth AOA positioning technology has become the recommended choice for car keys due to its advantages. Bluetooth AOA positioning should not be limited to angle estimation, further the critical aspect is to apply this technology in different fields, identify shortcomings through practical applications, and continuously enhance its capabilities.

The most important thing in AOA estimation is the antenna array. The antenna unit must ensure accurate signal processing, switching, impedance matching, etc. These are issues that need to be carefully designed. The problem of multipath is also a major challenge faced by AOA estimation. Nowadays, AI technology has the capability to process signals, which raises the question of its potential application. The work done so far is of certain significance, however, it also has its shortcomings that need to be addressed in future research. In conclusion, Bluetooth AOA is a reliable and valuable technology that deserves further investigation. By constantly addressing hardware and multipath issues, we can enhance the practical applications of this technology in our daily lives.

ACKNOWLEDGMENT

The author would like to express gratitude to Nodic company for their technical support provided in the forum. Furthermore, the editor of IEEE Sensor Journal deserve appreciation for their assistance and guidance. The author is also thankful to the all reviewers for their valuable comments on the paper revision. Finally, the author acknowledges LetPub(www.letpub.com) for their editing service, which significantly enhanced the quality of the paper.

REFERENCES

[1] Z. Wang, Z. Yang, and T. Dong, "A Review of Wearable Technologies for Elderly Care that Can Accurately Track Indoor Position, Recognize Physical Activities and Monitor Vital Signs in Real Time," *Sensors*, vol. 17, no. 2, pp. 341-346, 2017.

[2] L. Kajdocsi, A. Dörömbözi and J. Kovács, "Development of Bluetooth Mesh Core Stack using OmNET++," *2019 IEEE 17th International Symposium on Intelligent Systems and Informatics (SISY)*, 2019, pp. 23-28.

[3] G. Avitabile, A. Florio and G. Coviello, "Angle of Arrival Estimation through a Full-Hardware Approach for Adaptive Beamforming," in *IEEE Transactions on Circuits and Systems II: Express Briefs*., vol. 99, 2020.

[4] S. Monfared, A. Delepaut, M. Van Eeckhaute, P. De Doncker and F.Horlin, "Iterative Localization Method Using AoA for IoT Sensor Networks," *2019 IEEE 89th Vehicular Technology Conference (VTC2019-Spring)*, Kuala Lumpur, Malaysia, 2019, pp. 1-6.

[5] C. Huang, Y. Zhuang, H. Liu, J. Li, and W. Wang, "A performance evaluation framework for direction finding using BLE AoA/AoD receivers,"*IEEE Internet Things J.*, vol. 8, no. 5, pp. 3331–3345, Mar. 2021.

[6] P. Zand, J. Romme, J. Govers, F. Pasveer, and G. Dolmans, "A highaccuracy phase-based ranging solution with Bluetooth low energy (BLE)," in *Proc. IEEE Wireless Commun. Netw. Conf. (WCNC)*, Apr. 2019, pp. 1–8.

[7] B. Friedlander, "A sensitivity analysis of the MUSIC algorithm," *IEEE Trans. Acoust., Speech Signal Process.*, vol. 38, no. 10, pp. 1740–1751, Oct. 1990.

[8] T. Wang, H. Zhao, and Y. Shen, "An efficient single-anchor localization method using ultra-wide bandwidth systems," *Appl. Sci.*, vol. 10, no. 1, pp. 133-169, Jan. 2020.

[9] N. B. Suryavanshi, K. V. Reddy, V. R. Chandrika, "Direction Finding Capability in Bluetooth 5.1 Standard," *in International Conference on Ubiquitous Communications and Network Computing*, 2019, pp. 53-65.

[10] Z. HajiAkhondi-Meybodi, M. Salimibeni, A. Mohammadi and K. N. Plataniotis, "Bluetooth Low Energy and CNN-Based Angle of Arrival Localization in Presence of Rayleigh Fading," *2021 IEEE International Conference on Acoustics, Speech and Signal Processing (ICASSP)*, Toronto, ON, Canada, 2021, pp. 7913-7917.

[11] F. A. Toasa, L. Tello-Oquendo, C. R. Peñafiel-Ojeda and G. Cuzco, "Experimental Demonstration for Indoor Localization Based on AoA of Bluetooth 5.1 Using Software Defined Radio," *2021 IEEE 18th Annual Consumer Communications and Networking Conference (CCNC)*, Las Vegas, NV, USA, 2021, pp. 1-4.

[12] H. Yen et al., "I/Q Density-based Angle of Arrival Estimation for Bluetooth Indoor Positioning Systems," *2021 IEEE 93rd Vehicular Technology Conference (VTC2021-Spring) IEEE*, 2021.

[13] Z. Hajiakhondi-Meybodi, M. Salimibeni, K. N. Plataniotis, and A. Mohammadi, "Bluetooth low energy-based angle of arrival estimation via switch antenna array for indoor localization," in *Proc. IEEE 23rd Int. Conf. Inf. Fusion (FUSION)*, Jul. 2020, pp. 1–6.

[14] P. Mohaghegh, A. Boegli and Y. Perriard, "New Design of Antenna Array for Bluetooth Direction Finding," *2022 25th International Conference on Electrical Machines and Systems (ICEMS)*, Chiang Mai, Thailand, 2022, pp. 1-6.

[15] N. Paulino and L. M. Pessoa, "Self-Localization via Circular Bluetooth 5.1 Antenna Array Receiver," *IEEE Access.*, vol. 11, pp. 365-395, 2023.

[16] D. Xiao, S. Hu, K. Kang and H. Qian, "An Improved AoA Estimation Algorithm for BLE System in the Presence of Phase Noise," *IEEE Trans. Consum Electr.*, vol. 69, no. 3, pp. 400-407, Aug. 2023.

[17] Z. Liu, W. Dai, and M. Z. Win, "Mercury: An infrastructure-free system for network localization and navigation," *IEEE Trans. Mobile Comput.* ,vol. 17, no. 5, pp. 1119–1133, May. 2018.

[18] S. Mehryar et al., "Belief condensation filtering for rssi-based state estimation in indoor localization," in Proc. *IEEE Int. Conf. Acoust., Speech and Signal Process.*, May. 2019, pp. 8385–8389.

[19] P. Zand et al., "A high-accuracy phase-based ranging solution with Bluetooth Low Energy (BLE)," in Proc. *IEEE Wireless Commun. Netw.Conf.*, Apr. 2019, pp. 1–8.

[20] S. Mazuelas, Y. Shen, and M. Z. Win, "Spatiotemporal information coupling in network navigation," *IEEE Trans. Inf. Theory.*, vol. 64, no. 12, pp. 7759–7779, Dec. 2018.

[21] X. Qiu, B. Wang, J. Wang, and Y. Shen, "AoA-based BLE localization with carrier frequency offset mitigation," in *Proc. IEEE Int. Conf.Commun. Workshops (ICC Workshops)*, pp. 1–5, Jun. 2020.

[22] N. H. Nguyen, K. Do ganc¸ay, and E. E. Kuruoglu, "An iteratively reweighted instrumental-variable estimator for robust 3-D AoA localization in impulsive noise," *IEEE Trans. Signal Process.*, vol. 67, no. 18, pp. 4795–4808, Sep. 2019.

[23] M. Al-Sadoon et al., "A new low complexity angle of arrival algorithm for 1D and 2D direction estimation in MIMO smart antenna systems," *Sensors, vol.* 17, no. 11, pp. 2631-2633, Nov. 2017.

[24] M. Cominelli, P. Patras, and F. Gringoli. Dead on Arrival: An Empirical Study of The Bluetooth 5.1 Positioning System. *In Proceedings of the 13th International Workshop on Wireless Network Testbeds, Experimental Evaluation and Characterization (WiNTECH '19)*, 2019, pp. 13–20.
[25] M. Q. Kuisma. Whiteboard Web:I/Q Data for Dummies. Available: http://whiteboard.ping.se/SDR/IQ. Accessed on: April 24 2023.
[26] M. Wooley. (2019). *Bluetooth Direction Finding: A Technical Overview*. [Online] Available: https://www.bluetooth.com/bluetooth-resources/bluetooth-direction-finding/. Accessed on: April 24 2023.
[27] Q. Yan, J. Chen, G. Ottoy, and L. D. Strycker, "Robust AoA based acoustic source localization method with unreliable measurements," *Signal Process.*, vol. 152, pp. 13–21, Nov. 2018.
[28] W. Xiong, C. Schindelhauer, H. C. So, D. J. Schott, and S. J. Rupitsch, "Robust TDOA source localization based on Lagrange programming neural network," *IEEE Signal Process. Lett.*, vol. 28, pp. 1090–1094, 2021.
[29] T.-K. Le and K. C. Ho, "Joint source and sensor localization by angles of arrival," *IEEE Trans. Signal Process.*, vol. 68, pp. 6521–6534, 2020.
[30] S. Wu, S. Zhang, K. Xu, and D. Huang, "Probability weighting localization algorithm based on NLOS identification in wireless network," *Wireless Commun. Mobile Comput.*, vol. 11, 2019.
[31] A. Gabbrielli et al., "Anecho suppression delay estimator for angle of arrival ultrasonic indoor localization," *IEEE Trans. Instrum. Meas.*, vol. 70, pp. 1–12, 2021.
[32] A. Alma'aitah, B. Alsaify, and R. Bani-Hani, "Three-dimensional empirical AoA localization technique for indoor applications," *Sensors.*, vol. 19, no. 24, pp. 5544, Dec. 2019.
[33] H. Ye, B. Yang, Z. Long and C. Dai, "A Method of Indoor Positioning by Signal Fitting and PDDA Algorithm Using BLE AoA Device," *IEEE Sensors Journal.*, vol. 22, no. 8, pp. 7877-7887, Apr. 2022.

Wenzhao Shu received the B.S. degree in mechanical engineering from Yangtze University, Hubei, China, in 2021 and is currently pursuing the M.S. degree in mechanical engineering at YanShan University, Hebei, China. He is now participating in the joint training of Dongguan famous University joint training base, and carrying out project research in Guangdong Robotics Laboratory. He is currently involved in enterprise projects focused on Bluetooth AOA multi-target scenario applications. His research interests include Indoor localization, Bluetooth AoA, antenna array, signal processing and wireless communication.